ELSEVIER

Biophysical Chemistry 88 (2000) 11–34

Biophysical Chemistry

www.elsevier.nl/locate/bpc

Porphyrin-Fe(III)-hydroperoxide and porphyrin-Fe(III)-peroxide anion as catalytic intermediates in cytochrome P450-catalyzed hydroxylation reactions: a molecular orbital study

Olga Zakharieva[a,*], Alfred X. Trautwein[a], Cees Veeger[b]

[a] *Institute of Physics, Medical University Lübeck, 23538 Lübeck, Germany*
[b] *Laboratory of Biochemistry, Agricultural University, Dreijenlaan 3, 6703 HA Wageningen, The Netherlands*

Received 12 May 2000; received in revised form 7 July 2000; accepted 20 July 2000

Abstract

The hydroxylation of fluorobenzene and aniline, catalyzed by the porphyrin-Fe(III)-peroxide anion with either a cysteinate- or a histidyl-type of axial ligand as well as the hydroxylation of fluorobenzene, catalyzed by porphyrin-Fe(III)-hydroperoxide with a cysteinate-type of axial ligand as catalytic intermediates, have been investigated by electronic structure calculations in local spin-density approximation. Non-repulsive potential curves are, in contrast with porphyrin-Fe(III)-hydroperoxide, obtained only in the case of porphyrin-Fe(III)-peroxide anion as catalytic intermediate. The mutual substrate–porphyrin orientation with a dihedral angle between the plane of the substrate and the porphyrin plane of 45° is more favorable compared with the parallel orientation between these two planes. This orientation differs for the case of fluorobenzene hydroxylation from the corresponding one calculated by us with the ferryl-oxo-π-cation radical complex as a catalytic intermediate. The calculated reaction profiles show also the effectiveness of the histidyl-type coordinated porphyrin-Fe(III)-peroxide involved in P450 type of hydroxylation reactions. The calculations demonstrate the predominant role of the O_1–O_2 moiety of the porphyrin-Fe(III)-peroxide anion in the hydroxylation process of the substrates. The results indicate that the porphyrin-Fe(III)-peroxide anion is an effective catalytic species in hydroxylation reactions. In all the studied cases irrespective of the substrate and the nature of the axial ligand, the potential curves reach minimum at approximately 130–140 pm, expressing the length of an aromatic C–O bond.

Keywords: Cytochrome P450; Porphyrin-Fe(III)-(hydro)peroxide anion; Ferryl-oxo-π-cation radical; Molecular orbital calculations; Hydroxylation

Abbreviations: P450, cytochrome P450; Oxenoid-iron, ferryl-oxo-π-cation radical; (Hydro)peroxo-iron, porphyrin-Fe(III)-(hydro)peroxide anion

* Corresponding author. Fax: +49-451-500-4214.
E-mail address: zakharieva@physik.mu-luebeck.de (O. Zakharieva).

0301-4622/00/$ - see front matter
PII: S0301-4622(00)00194-0

1. Introduction

Cytochromes P450 catalyze the conversion of a large variety of aromatic and aliphatic compounds in what is considered to be a monooxygenation reaction. With the increase in the number of biologically important conversions, specifically (de)toxification and drug metabolism, the interest has been focused for many years towards the mechanism of catalysis of P450, to identify the catalytic species of Fe(III)-porphyrins responsible for a specific conversion. However, the ultimate catalytic intermediate has never been firmly identified. Sono et al. [1] have summarized the general

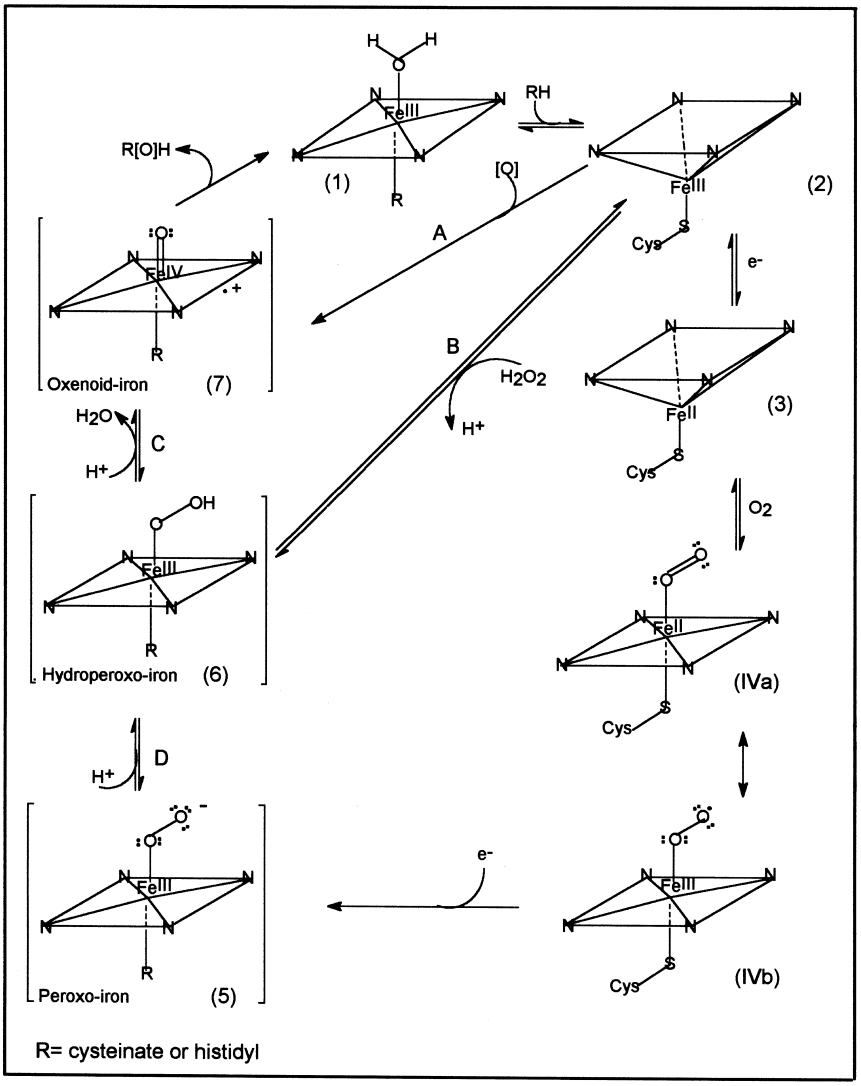

Fig. 1. Catalytic cycle of cytochrome P450 or cytochrome P450-type of reactions (adapted from Sono et al. [1]). Cytochrome P450-type of reactions are catalyzed with histidine as the axial ligand. For the different states of intermediates see Sono et al. [1]. It has been calculated that intermediate seven can catalyze the conversion into intermediate 1 [2,3]. The reversibility of reactions B and C have been demonstrated [4,5].

views with respect to the catalytic cycle of P450, which is given in an adapted view in Fig. 1 [2–5].

The general consensus, mostly based on chemical model studies [6–8], is that the actual catalytic species is the hypothetical so-called oxenoid-iron and supposed to be identical with horseradish peroxidase compound I (ferryl-oxo-π-cation radical or oxenoid-iron). In addition, a horseradish compound II intermediate has been postulated [9], but it has not been identified. Preliminary efforts identifying the oxenoid-iron intermediate have been reported [10,11].

Support for a role of oxenoid-iron as a possible catalytic intermediate comes from molecular orbital studies of Zakharieva et al. [2,3] in which it is demonstrated that this form could act as a catalyst in P450-type chemistry. The calculations show regio-selectivity of attack in qualitative agreement with the experimental observations. However, the calculated energy barriers are rather high. On the other hand, although the existence of the $[PorFr(III)O_2]^-$ type of intermediate (peroxo-iron) is accepted (Fig. 1) [1,12–14], its catalytical role is denied and attributed to the oxenoid-iron intermediate [15]. This is despite the X-ray structure of a thiolate-Heme Fe(II)-O_2 model [16] and the preparation and characterization of a large number of model compounds [17,18]. Balch [19] has given spectroscopic characteristics of the peroxo-iron model and claims that there are no published reports documenting the conversion of this compound into the oxenoid-iron intermediate. Recently, Dawson et al. [20] postulated $PorFe(II)O_2$ as a catalytic intermediate, but they consider it to be an ineffective oxidant.

The first experimental indication for the existence of a peroxide-type of intermediate is reported by McDonald et al. [21]. Upon reaction of P450 with ^{18}O-labeled iodobenzene fast exchange of oxygen takes place with $H_2^{18}O$. By this reaction the oxenoid-iron is formed (reaction A, Fig. 1), which by reversible H_2O addition is converted into hydroperoxo-iron or by abstracting an extra H^+ into peroxo-iron. Despite this, the authors maintained the view of oxenoid-iron as the catalytic intermediate. Evidence for a functional role of different Fe-(per)oxo species is presented by Vaz et al. [22] to account for differences in reaction rates of olefinic substrates by different P450s, as well as for the oxidative deformylation of aldehydes to olefins and formate [23–26]. In fact the Coon group proposes peroxo-iron as a nucleophilic intermediate (aldehyde deformylation); hydroperoxo-iron, as a nucleophilic or electrophilic intermediate (aldehyde deformylation, epoxidation) and oxenoid-iron as an electrophilic intermediate (hydroxylation and epoxidation). (Hydro)peroxo-iron as an intermediate in P450-type reactions is experimentally proposed in the study with MP-8 [4,5,27]. MP-8 is a heme-containing mini-enzyme of eight amino acids derived from cytochrome *c* and contains a tightly bound histidine in the axial position. It is able to catalyze both peroxidase-types and P450-types of reactions.

In order to understand in more detail the process of oxygen incorporation by P450-type of chemistry it is essential to extend our previous approach by investigating the reaction pathways of the peroxo-iron anion and hydroperoxo-iron in hydroxylation reactions by means of molecular orbital calculations in local spin-density approximation [28]. The aim of this paper is to elucidate their possible involvement as catalytic intermediates, as well as to determine the orbital interactions during the primary reaction step, the reasons for the cleavage of the O_1–O_2 bond and the mechanism of the reaction. The heme system and the substrate are explicitly included in the calculations.

2. Procedure and methods

It has recently been shown that the energetics of chemical reactions can theoretically be described by local density functional methods with results comparable with or even better than those of Hartree–Fock calculations including many body perturbation corrections up to fourth order [29,30]. These calculations were performed by defining a certain reaction coordinate, followed by full geometry optimization along that coordinate, and proving the transition state by vibrational

analysis. However, an analogous procedure would be prohibitive in the case of the reactions investigated in this work because the whole system consisting of substrate and the peroxo-iron ($[PorFe(III)O_2]^-$) contains 58 atoms with 171 valence orbitals (cysteinate-type axial ligand) and 62 atoms with 184 valence orbitals (histidyl-type axial ligand), and is an open-shell system requiring spin-polarized calculations. Moreover, a large number of iterations is generally needed until convergence of electron density is achieved, because the occupied and empty orbitals are energetically not well separated from each other. For these reasons, a full geometry optimization along the reaction coordinate is not feasible, so that the main purpose of these investigations consists of understanding, at least qualitatively, the changes which the two interacting systems undergo during the hydroxylation and how the final state is reached. Previous calculations on the hydroxylation of monofluorobenzene [2] and substituted anilines [3] by oxenoid-iron have shown that valuable insight into the reaction mechanisms can be gained even without full geometry optimization along the reaction coordinate.

The molecular orbital calculations have been performed within the local density approximation [31–33] by the self-consistent (SCC)-Xα method [28]. As a whole, the (SCC)-Xα code is more than an order of magnitude faster than the Xα option of Gaussian 98 and requires substantially less memory space. For these reasons this method is particularly suited for describing the electronic properties of large molecules containing transition metal atoms as shown by application on systems of biological relevance [34] as well as on the investigation of reaction pathways [2,3]. The latter results show regio-selectivity of attack in agreement with the experimental observations in vivo [35,36].

Only the geometry optimization of the catalytic center-peroxo-iron is performed with the three-parameter gradient-corrected density functional method B3LYP with a 3-21G basis set [37]. These calculations were very time consuming and have shown again that a full geometry optimization for each step along the reaction coordinate is not feasible with this method.

3. Geometrical assumption

The geometry optimization of peroxo-iron with H_3CS^- as axial ligand, using the three-parameter gradient-corrected density functional method B3LYP with 3-21G basis set, shows the following parameters. The iron–sulfur distance is determined as 235 pm in accordance with the EXAFS data for the low-spin ferric P450cam [12] as well as with the X-ray structure of a model dioxygen P450 heme complex [16,38]. The sulfur atom is tilted by 6.8° out of the porphyrin normal direction towards the positive *x*-axis. The iron–nitrogen distance is obtained as 199 pm, the $Fe–O_1$ and $O_1–O_2$ distances as 189 and 140 pm, respectively. An asymmetric bent, end-on structure with only one oxygen directly bound to the iron is obtained in accordance with [14,39]. The FeO_1O_2 plane is found along the bisector of the N_1FeN_2 right angles of the equatorial porphyrin plane, the so-called 'staggered' structure, in good agreement with the results shown by Dedieu et al. [39]. This orientation minimizes the steric contacts between the distal oxygen O_2 and the pyrrole nitrogens. The angle $Fe–O_1–O_2$ is obtained as 116°.

Together with peroxo-, also hydroperoxo-iron is modeled. For the calculations with histidyl-type axial ligand the geometry parameters already used in our previous work [2] are taken. The gas phase geometries used for the substrate molecules (fluorobenzene and aniline) are from Hellwege and Hellwege [40].

A major problem in studying reactions of this type is the lack of experimental data for the intermediate sections of the potential surfaces and for the geometry of the transition state. In the course of the reaction both the substrate and the porphyrin undergo deformations. The stepwise deformation of the substrate leads to a transition state geometry as calculated by Korzekwa et al. [41]. The next neighbor bond of the carbon under attack (C_4, position *para* with respect to F or NH_2, see Fig. 2) are elongated stepwise, namely from 138.3 to 152.5 pm (fluorobenzene), from 139.2 to 152.5 pm (aniline), $C_4–H$ from 108.1 to 113.6 pm (fluorobenzene) and from 108.4 to 113.6 pm (aniline). The hydrogen atom in both cases is

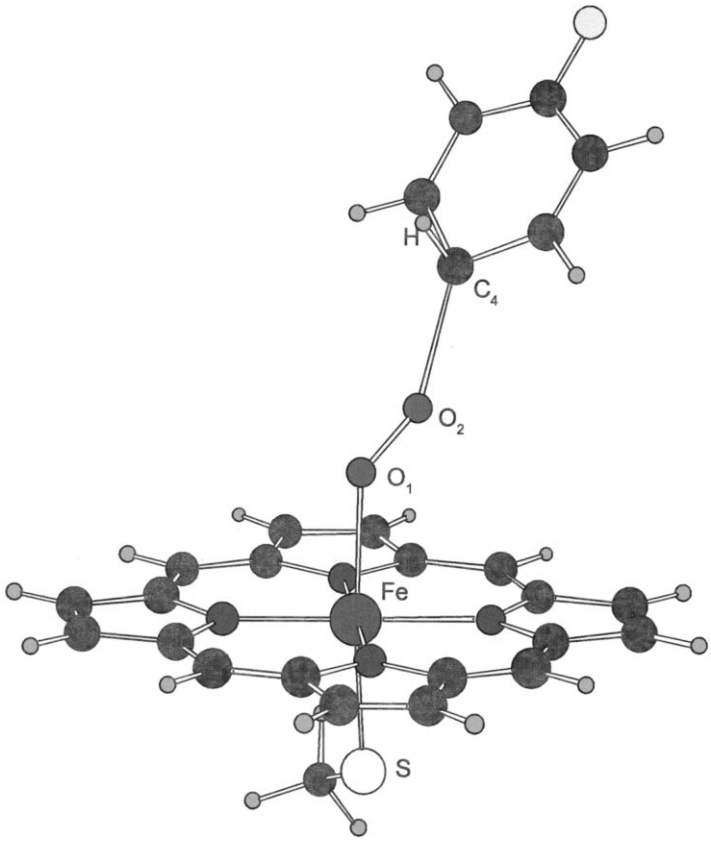

Fig. 2. Geometrical arrangement of the substrate-porphyrin system for the reaction of fluorobenzene hydroxylation with cysteinate-type coordinated peroxo-iron, attack on para-position with respect to NH_2.

pushed out of the substrate plane so that the carbon atom under attack approaches a state being near to tetrahedral symmetry.

The stepwise deformation of the catalytic intermediate is modeled with the elongation of the $Fe–O_1$ and $O_1–O_2$ bond lengths from 189 to 226 and from 140 to 170 pm, respectively. The Fe–S distance is kept constant and the porphyrin core is assumed to remain planar. The assumed reaction coordinate is the $C_4–O_2$ distance representing the bond to be formed during the hydroxylation.

In a search of a possible hydroxylation reaction pathway different investigations have been performed with regards to the character of the catalytic center, the kind of the substrate, the substrate orientation towards the porphyrin and the projection of the $O_1–O_2$ bond on the porphyrin plane.

4. Search for a possible reaction pathway

4.1. Hydroperoxo-iron as a catalytic center

All the obtained potential curves when varying: (i) the direction of substrate approach, namely along the negative as well as the positive *x*-axis; (ii) the dihedral angle between the planes defined as FeO_1O_2 and $O_1O_2H_p$; (iii) the valent- and spin-state of iron; (iv) the projection of $O_1–O_2$ in the porphyrin plane — along the $Fe–N_1$ bond or along the bisector of the N_1FeN_2 angle have not shown any attractive interaction. According to

this only peroxo-iron as catalytic center will be considered in the following discussions.

4.2. Peroxo-iron as catalytic center

With the parallel orientation of the substrate and the porphyrin plane the obtained potential curves are either very flat (the cases of fluorobenzene and aniline hydroxylation with cysteinate-type coordinated peroxo-iron (Figs. 3a,b) or there is no attractive interaction at all — the case of aniline hydroxylation and histidyl-type catalytic intermediate.

With a substrate plane rotated about an axis through C_4 and parallel to the *y*-axis at 45° and a projection of O_1–O_2 in the porphyrin plane along the bisector of the N_1FeN_2 angle a well expressed attractive interactions are obtained for fluorobenzene (Fig. 4a) and aniline (Fig. 4b) hydroxylations with cysteinate-type coordinated peroxo-iron as catalytic intermediate as well as for aniline hydroxylation with histidyl-type peroxo-iron (Fig. 5). The substrate molecule approach is parallel to the bisector of the N_1FeN_2 right angle of the equatorial porphyrin plane. The mutual orientation between the catalytic center peroxo-iron and the substrate is shown in Fig. 2 for the hydroxylation reaction of fluorobenzene. The maxima of the potential curves are at 200 pm (fluorobenzene hydroxylation), 190 pm (aniline hydroxylation) and 181 pm (aniline hydroxylation and histidyl-type catalytic intermediate). Varying the position of the FeO_1O_2 plane, the substrate molecule, its orientation towards the peroxo-iron, the following results are obtained:

1. The cysteinate-type peroxo-iron-substrate system is more stabilized and the hydroxylation reaction proceeds easier with fluorobenzene when the projection of the O_1–O_2 bond lies on the bisector of the N_1FeN_2 right angle of the porphyrin plane although the rotation of the O_1–O_2 bond in the peroxo-iron bend-on configuration is nearly free.
2. The whole system is stabilized in the range

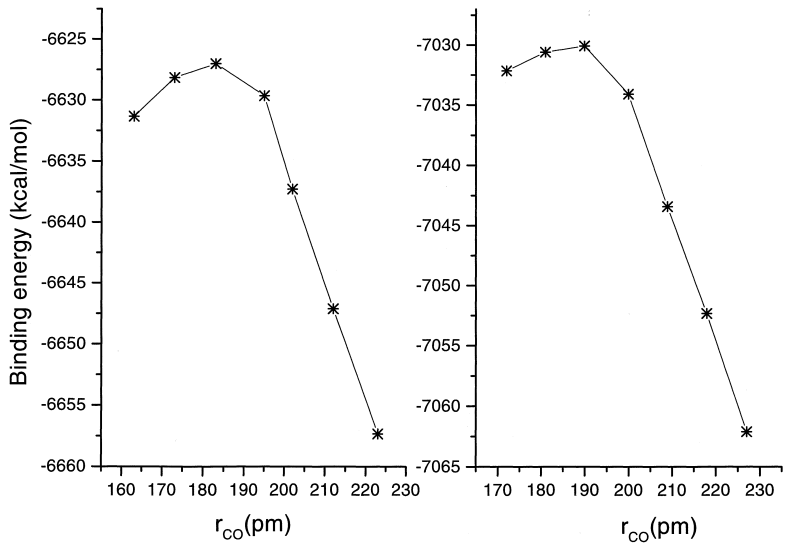

Fig. 3. (a) Changes in binding energies for the reaction of monofluorobenzene hydroxylation with cysteinate-type coordinated peroxo-iron, attack on para-position with respect to F with parallel orientation of the substrate and the porphyrin plane, as a function of the C–O distance. (b) Changes in binding energies for the reaction of aniline hydroxylation with cysteinate-type coordinated peroxo-iron, attack on para-position with respect to NH_2 with parallel orientation of the substrate and the porphyrin plane, as a function of the C–O distance.

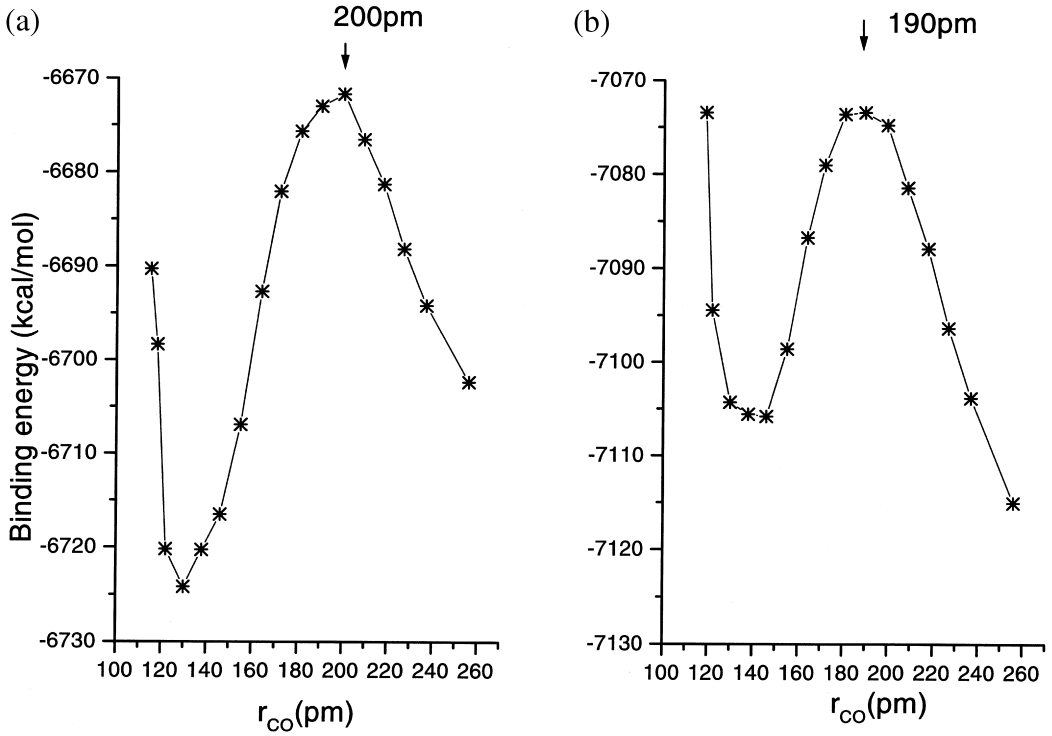

Fig. 4. (a) Changes in binding energies for the reaction of monofluorobenzene hydroxylation with cysteinate-type coordinated peroxo-iron, attack on para-position with respect to F with mutual substrate-catalytic center orientation, shown in Fig. 2, as a function of the C–O distance. (b) Changes in binding energies for the reaction of aniline hydroxylation with cysteinate-type coordinated peroxo-iron, attack on para-position with respect to NH_2 with mutual substrate-catalytic center orientation, shown in Fig. 2, as a function of the C–O distance.

40–45 kcal/mol in the case of the rotated substrate molecule.

3. With the parallel substrate orientation towards the porphyrin plane an attractive interaction aniline-catalytic center is obtained only in the case of the cysteinate-type peroxo-iron but not in the case of histidyl-type peroxo-iron as catalytic intermediate.
4. The potential curves for the rotated substrate orientation (Fig. 3a,b) have shown a well expressed maxima.
5. The energy barriers are considerably smaller in the substrate rotated cases.
6. An attractive interaction is obtained in the case of fluorobenzene hydroxylation by the rotated orientation for C_4–O_2 distances shorter than 200 pm while in the case of parallel substrate orientation towards the porphyrin plane the corresponding attractive interaction is obtained at a considerably shorter value, namely 183 pm.
7. Not only the maximum, but also the following minimum is well expressed in the rotated case, while in the potential curves corresponding to the parallel orientation of the substrate and the porphyrin plane no more points can be calculated for reaction coordinate values smaller than 163 pm (fluorobenzene) and 173 pm (aniline), respectively. The reason is that the highest occupied molecular orbitals/lowest unoccupied molecular orbitals (HOMO/LUMO) levels in the parallel orientation are almost degenerate causing severe difficulties concerning the convergence.

Table 1
Changes of effective charges for the reaction of: (a) fluorobenzene with cysteinate-type coordinated peroxo-iron (attack on para-position with respect to F); (b) aniline with cysteinate-type coordinated peroxo-iron (attack on para-position with respect to NH_2)

	(a) Fluorobenzene							
r_{OC}	Q(Fe)	$Q(O_1)$	$Q(O_{2)}$	Q(S)	$Q(C_4)$	Q(F)	Q(H)	Q(sub)[b]
inf[a]	0.953	−0.426	−0.414	−0.306	−0.137	−0.187	0.023	–
256	0.967	−0.429	−0.410	−0.310	−0.032	−0.212	−0.010	−0.039
237	0.968	−0.429	−0.405	−0.310	−0.020	−0.215	−0.015	−0.057
227	0.968	−0.429	−0.403	−0.311	−0.008	−0.216	−0.017	−0.057
218	0.967	−0.433	−0.401	−0.315	0.007	−0.217	−0.018	−0.053
209	0.964	−0.443	−0.402	−0.319	0.028	−0.217	−0.017	−0.029
200[c]	0.961	−0.458	−0.403	−0.322	0.056	−0.217	−0.016	0.008
190	0.957	−0.476	−0.403	−0.323	0.091	−0.218	−0.014	0.088
181	0.955	−0.493	−0.400	−0.324	0.126	−0.218	−0.011	0.092
172	0.957	−0.505	−0.398	−0.324	0.157	−0.218	−0.010	0.119
164	0.958	−0.513	−0.397	−0.325	0.181	−0.220	−0.010	0.137
155	0.959	−0.515	−0.394	−0.324	0.195	−0.221	−0.010	0.140
146	0.956	−0.513	−0.383	−0.324	0.199	−0.222	−0.010	0.127
138	0.954	−0.509	−0.359	−0.325	0.197	−0.224	−0.010	0.107
130	0.947	−0.502	−0.330	−0.328	0.192	−0.224	−0.006	0.094
122	0.937	−0.494	−0.294	−0.334	0.186	−0.224	0.0	0.090
118	0.931	−0.485	−0.302	−0.337	0.180	−0.224	0.018	0.096
115	0.924	−0.478	−0.283	−0.342	0.178	−0.224	0.026	0.099
	(a) Aniline							
r_{OC}	Q(Fe)	$Q(O_1)$	$Q(O_2)$	Q(S)	$Q(C_4)$	$Q(N_{an})$	Q(H)	Q(sub)[b]
inf[a]	0.953	−0.426	−0.414	−0.306	−0.124	−0.216	0.012	–
256	0.968	−0.430	−0.410	−0.313	−0.020	−0.224	−0.022	−0.019
237	0.969	−0.430	−0.406	−0.314	−0.007	−0.226	−0.026	−0.029
227	0.968	−0.431	−0.404	−0.317	0.003	−0.227	−0.026	−0.029
218	0.967	−0.435	−0.404	−0.321	0.017	−0.227	−0.026	−0.016
209	0.964	−0.444	−0.406	−0.325	0.037	−0.227	−0.026	0.014
200	0.960	−0.458	−0.408	−0.329	0.063	−0.227	−0.024	0.055
190[c]	0.957	−0.476	−0.410	−0.331	0.094	−0.227	−0.022	0.104
181	0.956	−0.494	−0.410	−0.332	0.127	−0.227	−0.019	0.144
172	0.960	−0.506	−0.407	−0.332	0.157	−0.229	−0.017	0.170
164	0.960	−0.514	−0.406	−0.332	0.180	−0.228	−0.016	0.186
155	0.961	−0.517	−0.401	−0.332	0.193	−0.230	−0.014	0.189
146	0.959	−0.516	−0.389	−0.333	0.198	−0.231	−0.011	0.181
138	0.953	−0.512	−0.364	−0.336	0.196	−0.231	−0.006	0.172
130	0.945	−0.510	−0.333	−0.341	0.192	−0.231	0.005	0.170
122	0.933	−0.498	−0.296	−0.350	0.188	−0.231	0.022	0.176
119	0.928	−0.493	−0.303	−0.351	0.180	−0.231	0.034	0.183

[a] Separated systems with deformed structures (see the text).
[b] Molecular charge of the substrate.
[c] Corresponds to the maximum of the potential curve.

According to these results we consider the rotated substrate orientation towards the porphyrin plane as favorable. Only the results for this orientation and a substrate approach parallel to the bisector of the N_1FeN_2 angle will be discussed in the following sections.

Table 2
Changes of effective charges for the reaction of aniline with the histidyl-type coordinated peroxo-iron (attack on para-position with respect to NH_2)[a]

r_{OC}	Q(Fe)	$Q(O_1)$	$Q(O_2)$	$Q(N_{imi})$	$Q(N_1)$	$Q(C_4)$	$Q(C_1)$	$Q(N_{an})$	Q(H)	Q(sub)[b]
inf[a]	0.858	−0.366	−0.348	−0.173	−0.211	−0.124	0.039	−0.216	0.007	–
256	0.872	−0.381	−0.355	−0.174	−0.240	−0.025	0.042	−0.216	−0.003	0.103
237	0.872	−0.388	−0.357	−0.174	−0.215	−0.029	0.045	−0.215	−0.001	0.104
218	0.875	−0.400	−0.361	−0.175	−0.216	0.029	0.045	−0.213	0.002	0.216
209	0.881	−0.408	−0.363	−0.176	−0.217	0.049	0.047	−0.213	0.003	0.250
200	0.888	−0.418	−0.365	−0.177	−0.219	0.074	0.049	−0.212	0.005	0.289
190	0.896	−0.432	−0.368	−0.179	−0.220	0.104	0.051	−0.212	0.007	0.335
181[c]	0.901	−0.448	−0.371	−0.182	−0.221	0.137	0.046	−0.212	0.011	0.380
172	0.903	−0.460	−0.371	−0.184	−0.222	0.166	0.045	−0.212	0.015	0.418
164	0.903	−0.468	−0.369	−0.186	−0.223	0.188	0.042	−0.211	0.018	0.445
155	0.901	−0.473	−0.366	−0.187	−0.224	0.203	0.041	−0.211	0.024	0.463
146	0.895	−0.476	−0.354	−0.189	−0.225	0.210	0.042	−0.211	0.030	0.481
138	0.885	−0.477	−0.330	−0.191	−0.226	0.211	0.043	−0.211	0.039	0.490
130	0.872	−0.476	−0.300	−0.193	−0.227	0.210	0.043	−0.211	0.052	0.500
122	0.855	−0.471	−0.263	−0.196	−0.228	0.208	0.044	−0.211	0.072	0.509
115	0.847	−0.474	−0.218	−0.208	−0.230	0.209	0.042	−0.213	0.102	0.521

[a] For details of footnotes see Table 1.

Table 3
Changes of spin-density for the reaction of: (a) fluorobenzene with cysteinate-type coordinated peroxo-iron (attack on para-position with respect to F); (b) aniline with the cysteinate-type coordinated peroxo-iron (attack on para-position with respect to NH_2)

	(a) Fluorobenzene							
r_{OC}	Fe(3d)	S(3p)	O_1(2p)	O_2(2p)	C_4(2p)	C_{135}[b] (2p)	F(2p)	H(1s)
inf[a]	1.106	0.066	0.432	0.524	–	–	–	–
256	1.157	0.061	0.421	0.504	0.003	−0.018	–	−0.002
237	1.177	0.060	0.416	0.488	0.006	−0.024	–	−0.003
227	1.184	0.058	0.411	0.474	0.009	−0.021	–	−0.002
218	1.178	0.054	0.396	0.451	0.013	0.031	–	−0.002
209	1.156	0.057	0.359	0.412	0.013	0.073	0.002	0.004
200	1.121	0.067	0.298	0.349	0.002	0.218	0.006	0.015
190	1.068	0.076	0.222	0.270	−0.016	0.436	0.011	0.044
181	1.031	0.079	0.148	0.196	−0.026	0.642	0.017	0.069
172	1.037	0.076	0.091	0.133	−0.025	0.785	0.020	0.086
164	1.045	0.076	0.046	0.087	−0.023	0.870	0.023	0.100
155	1.059	0.079	0.012	0.055	−0.021	0.925	0.024	0.110
146	1.075	0.084	−0.010	0.038	−0.018	0.937	0.024	0.120
138	1.100	0.091	−0.022	0.029	−0.015	0.917	0.024	0.125
130	1.129	0.101	−0.026	0.024	−0.012	0.866	0.022	0.130
122	1.172	0.113	−0.024	0.023	−0.010	0.788	0.020	0.134
118	1.214	0.118	−0.013	0.034	−0.005	0.716	0.018	0.129
115	1.245	0.127	−0.008	0.035	−0.004	0.658	0.017	0.130

	(b) Aniline								
r_{OC}	Fe(3d)	O_1(2p)	O_2(2p)	S(3p)	N_1(2p)	C_{135}[b] 2p	C_4(2p)	N_{an}(2p)	H(1s)
inf[a]	1.106	0.432	0.524	0.066	−0.033	–	–	–	–
256	1.136	0.422	0.511	0.060	−0.034	−0.067	0.001	–	–
237	1.147	0.419	0.498	0.058	−0.032	−0.008	0.003	–	–
227	1.149	0.415	0.486	0.055	−0.031	−0.003	0.061	–	–
218	1.138	0.401	0.468	0.051	−0.028	0.020	0.011	–	–
209	1.120	0.370	0.437	0.053	−0.024	0.079	0.014	0.004	–
200	1.079	0.316	0.389	0.064	−0.020	0.190	0.008	0.008	0.015
190	1.038	0.245	0.322	0.076	−0.019	0.365	−0.008	0.015	0.035
181	1.021	0.170	0.248	0.083	−0.020	0.547	−0.020	0.022	0.057
172	1.041	0.104	0.173	0.083	−0.024	0.694	−0.025	0.028	0.076
164	1.061	0.046	0.110	0.083	−0.026	0.811	−0.027	0.032	0.093
155	1.084	0.003	0.066	0.089	−0.028	0.874	−0.027	0.033	0.106
146	1.110	−0.021	0.042	0.096	−0.028	0.887	−0.026	0.033	0.114
138	1.143	−0.031	0.030	0.106	−0.028	0.858	−0.024	0.031	0.118
130	1.184	−0.031	0.026	0.117	−0.027	0.794	−0.020	0.028	0.122
122	1.239	−0.026	0.028	0.133	−0.026	0.695	−0.017	0.024	0.125
119	1.274	−0.015	0.038	0.134	−0.027	0.632	−0.014	0.021	0.127

[a] For details see Table 1.
[b] 2p spin density on C_1, C_3, C_5 atoms of the substrate.

5. Charge and spin distribution in peroxo-iron ($[PorFe(III)O_2]^-$)–substrate complex

Qualitative insight into the reaction mechanism can be obtained by analyzing the changes in the charge- and spin-density distribution along the optimized reaction coordinate. The data are presented in Tables 1–4.

In the case of fluorobenzene hydroxylation at large separations (256–209 pm) the electron flow is towards the substrate. This is in contrast to our previous results for the hydroxylation of fluoro-

Table 4
Changes of overlap populations for the reactions: (A) fluorobenzene; (B) aniline with the cysteinate-type coordinated peroxo-iron; (C) the reaction of aniline with histidyl-type coordinated peroxo-iron

	(A)			(B)			(C)		
r_{OC}	O_1–O_2	O_2–C_4	C_4–H	O_1–O_2	O_2–C_4	C_4–H	O_1–O_2	O_2–C_4	C_4–H
inf[a]	0.532	–	0.686	0.532	–	0.686	0.547	–	0.686
256	0.533	–	0.633	0.531	−0.002	0.681	0.546	0.010	0.684
237	0.531	–	0.635	0.530	−0.003	0.683	0.543	0.020	0.685
227	0.529	0.003	0.637	0.528	0.002	0.684	0.540	0.033	0.686
218	0.526	0.013	0.640	0.525	0.009	0.686	0.537	0.043	0.686
209	0.520	0.037	0.642	0.520	0.030	0.688	0.531	0.064	0.687
200	0.512	0.080	0.644	0.512	0.068	0.689	0.524	0.098	0.688
190	0.499	0.150	0.645	0.499	0.131	0.689	0.512	0.155	0.687
181	0.482	0.237	0.644	0.483	0.212	0.686	0.496	0.231	0.685
172	0.458	0.346	0.640	0.462	0.315	0.679	0.478	0.328	0.677
164	0.436	0.459	0.631	0.439	0.431	0.666	0.458	0.436	0.665
155	0.418	0.567	0.617	0.420	0.541	0.648	0.442	0.541	0.647
146	0.406	0.662	0.602	0.408	0.636	0.629	0.429	0.635	0.627
138	0.376	0.755	0.586	0.399	0.725	0.608	0.420	0.722	0.603
130	0.389	0.839	0.568	0.390	0.806	0.582	0.409	0.801	0.579
122	0.380	0.922	0.544	0.380	0.876	0.553	0.398	0.872	0.549
118	0.313	0.975	0.539	0.308	0.934	0.531	0.380	0.938	0.510
115	0.280	1.015	0.523	0.275	0.960	0.522	0.290	0.981	0.500

[a] For details see Table 1.

benzene, catalyzed by oxenoid-iron (Compound I) [2]. Only near the maximum of the potential curve and later on in the region of its positive slope the calculated small electron flow changes its direction towards the catalytic center-cysteinate-type peroxo-iron. The maximum value of the total charge by the substrate is +0.140 at a very small value of the reaction coordinate, namely 155 pm (Table 1a), far away from the maximum of the potential curve.

In the case of aniline hydroxylation and the same catalytic intermediate again at large separations (256–218 pm) the electron flow is towards the substrate. At reaction coordinate 209 pm and later on an electron flow occurs from the substrate to the catalytic center (Table 1b). In [42] the authors propose mechanism for P450 dependent oxidative deformylation of aldehydes. After a nucleophilic attack by Fe(III)–O–O^- to the carbonyl group forming an intermediate, the electrons move in a concerted electrocyclic way towards the Fe(III), so, in the same direction as derived from our calculations.

Compared with the case of fluorobenzene hydroxylation discussed above the electron flow towards the catalytic center is higher because of the electron donating effect of the amino group. The same tendency is obtained by us also in the cases of 3-fluoro-methyl-aniline hydroxylation [3] when compared with monofluorobenzene hydroxylation with oxenoid-iron as catalytic center [2]. At the same time this electron flow for the reaction of aniline with cysteinate-type peroxo-iron is significant smaller when compared with the case of 3-fluoro-methyl-aniline hydroxylation catalyzed by oxenoid-iron [3]. The substrate becomes ionized with a total charge +0.104 at the maximum of the potential curve and +0.189 at a value 155 pm of the reaction coordinate (see Table 1b).

In the case of aniline hydroxylation and histidyl-type coordinated peroxo-iron the electron flow from the substrate towards the peroxo-iron is from the very beginning of the reaction (Table 2) and is stronger when compared with the hydroxylation reaction of aniline catalyzed by the cysteinate-type coordinated peroxo-iron (Table 1b). This difference between the histidyl- and the cysteinate-type of catalytic center concerning the same reaction, namely the hydroxylation of aniline is connected with the fact that the thiolate is the most and the histidyl is the least electron donating ligand. Accordingly, the total charge (Q_{sub}) of the substrate at the maximum of the potential curve in this case is +0.380 (Table 2), significantly higher in comparison with the case of aniline hydroxylation catalyzed by the cysteinate-type coordinated peroxo-iron with $Q_{sub} = +0.104$ at the maximum of the potential curve (Table 1b). Beyond the maximum with the decline of the reaction coordinate this charge increases further. According to this the histidyl-type coordinated peroxo-iron seems to be more prepared to act as an electrophilic center.

This electron flow in all cases discussed above determines the changes in the charge- and spin-density distribution in the whole system. The major changes are in the region where the reaction takes place, namely the carbon atom under attack (C_4) and the iron-bound peroxide. The charge of the carbon atom under attack increases rapidly, followed by the increase of the negative charge of O_1. The charge changes by O_2 are small compared to O_1 and only beyond the minimum of the potential curve O_2 charge changes increase. In some way O_2 can be considered as positive with respect to O_1. A substantial part from the substrate electron flow is coming to O_1. All the other atoms undergo minor changes.

In the substrate-free peroxo-iron the two unpaired electrons are located on the Fe(3d) orbital and on the antibonding π^* O_1–O_2 orbital. The higher spin-density on O_2 when compared with O_1 is a measure of O_2 reactivity. Along the reaction coordinate the major spin-changes are again connected with the both oxygen atoms (O_1 and O_2) as well as the substrate (Table 3). The significant diminishing of the spin density of the proximal and the distal oxygen atoms is connected with the strong stabilization of the unoccupied spin-down π^* O_1–O_2 orbital along the reaction in the occupied region discussed below by Walsh diagrams. There is also a small decline of the iron spin along the reaction coordinate. The induced spin in the substrate is almost exclusively located at the carbon atoms next and opposite to the site of attack. Similar to the results for

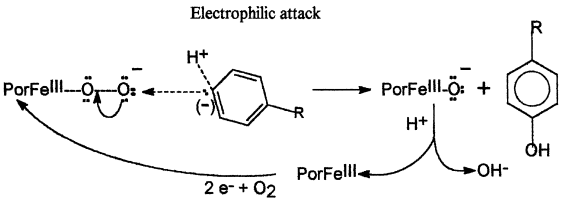

Scheme 1. According to the calculations in the electrophilic attack by peroxo-iron electrons move from the negatively charged tetrahedral carbon (H^+ leaving) to the distal O_2. At the same time electrons move from the distal O_2 to the proximal O_1. At the moment (approx. 140 pm) where the formed C–O bond is very strong O_1 has higher negative charge when compared with O_2. The catalytic intermediate is converted by the uptake of a H^+ contemporary into $PorFe^{III}$-hydroxide.

the hydroxylation, catalyzed by ferryl-oxo-π–cation radical complex [2] the substrate spin-density change is predominantly a polarization effect.

By the overlap population (Table 4) the reduction of the O_1–O_2 bond strength indicates the bond rupture and formation of $PorFe^{III}$-OH (Scheme 1). Concomitantly a strong O_2–C_4 bond is forming.

The effect of the histidyl-type proximal ligand on the electron distribution of the porphyrin consists in polarizing the $3d_{z2}$ orbital out of the porphyrin plane, toward the other axial ligand. This makes the $3d_{z2}$ orbital better prepared to interact with σ orbital of the O_1–O_2 moiety. As a result the overlap between the iron $3d_{z2}$ and the σ O_1–O_2 orbital increases, which in turn contributes to the strengthening of the Fe–O_1 bond. Also the O_1–O_2 bond is a little stronger in the case of histidyl-type proximal ligand in agreement with Nakamoto et al. [43] where the ν O_1–O_2 has been lowered by changing the axial ligand from imidazole to $SC_6H_5^-$. The latter is connected with the difference in the donating ability of both axial ligands. The electron donation from the cysteinate-type ligand to the iron facilitates later the π back-donation from Fe to O_1–O_2 where the electron flow occurs into an antibonding π* O_1–O_2 orbital which additionally decreases the O_1–O_2 bond strength. Therefore, the presence of a negatively charged thiolate can be expected to accentuate this effect.

6. Orbital interactions

6.1. Fluorobenzene and aniline hydroxylation-cysteinate-type coordinated peroxo-iron

The analysis of the changes in character and energy of the molecular orbitals involved in the reaction supplies additional important information about the reaction mechanism. Only the spin-down orbitals constituting the HOMOs and the LUMOs of the interacting systems need to be discussed. Analogous changes in character within the interacting spin-up orbitals do not influence the total energy because they are occupied.

The changes in the eigenvectors along the reaction pathway for the orbitals involved in these reactions are presented in Table S1, Fig. 7 (supplementary material, Appendix A) for the fluorobenzene hydroxylation and Table S2 (supplementary material, Appendix A) and Fig. 5, the Walsh

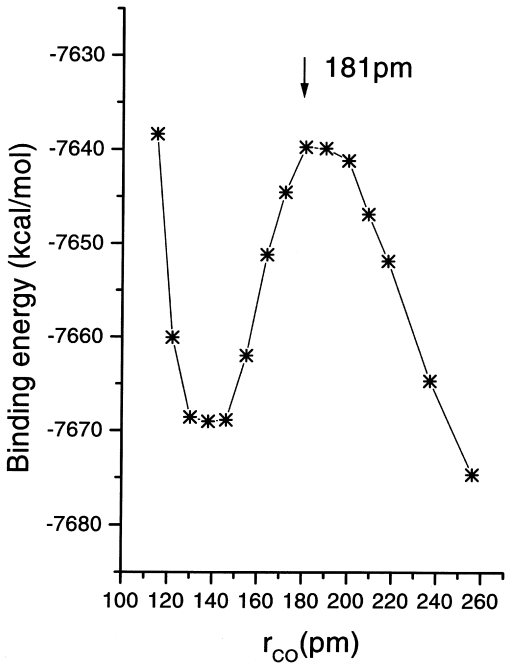

Fig. 5. Changes in binding energies for the reaction of aniline hydroxylation with histidyl-type coordinated peroxo-iron, attack on para-position with respect to NH_2 with mutual substrate-catalytic center orientation, shown in Fig. 2, as a function of the C–O distance.

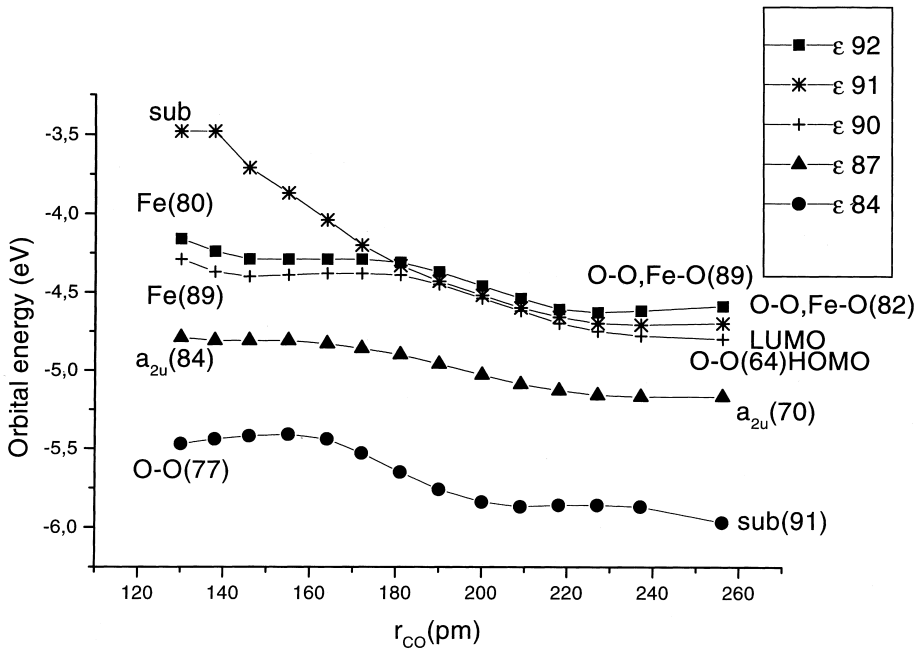

Fig. 6. Walsh diagram of the interacting spin-down molecular orbitals of the substrate-porphyrin system for the reaction of aniline hydroxylation at the para-position with respect to NH_2 with cysteinate-type coordinated peroxo-iron, as a function of the C–O distance.

diagram for the aniline hydroxylation. These orbitals at large separation are the HOMO p_z bonding orbital of the free fluorobenzene (MO no. 84) as well as of the free aniline denoted as 'Sub' in Tables S1 and S2 and Figs. 6 and 7, the HOMO of the whole system — an O_1–O_2 orbital (MO no. 90), the LUMO of the system (MO no. 91) — an Fe($d_{xz,yz}$) orbital, the LUMO^{+1} of the whole system (MO no. 92) — also an O_1–O_2 orbital. The a_{2u} orbital (MO no. 87) is also slightly involved as well as the MO no. 89. Because of the relatively short iron-pyrrole nitrogen bond distance (199 pm) the iron d_{x2-y2} orbital is destabilized in the LUMO region and does not play a role in this process.

Along the reaction pathway the substrate orbital (MO no. 84 at large separation) undergoes a strong destabilization and becomes unoccupied in the course of the reaction. On the way to the unoccupied region the substrate orbital shows a participation in a_{2u}, in HOMO, in LUMO and at a reaction coordinate 178 pm (fluorobenzene), 180 pm (aniline) when LUMO and LUMO^{+1} exchange their position LUMO^{+1} is the substrate orbital. In order words this destabilization is from MO no. 84 to MO no. 92. At the same time the initial substrate orbital transforms to an O_1–O_2 orbital.

A substantial role as substrate mediator are playing the following O_1–O_2 orbitals: the HOMO of the whole system at large separations (MO no. 90) and LUMO^{+1} (MO no. 92). The HOMO — a π^* antibonding O_1–O_2 orbital with a small admixture of σ bonding mediates at the beginning of the reaction the substrate orbital. With the decrease of the substrate eigenvectors later along the reaction coordinate this molecular orbital changes stepwise its character to an iron orbital with small contribution from O_1. The eigenvectors of O_1–O_2 at the end of the reaction are replaced by Fe. The latter changes are depicted on Fig. 8 for the case of aniline hydroxylation. Similar behavior is shown for the fluorobenzene hydroxylation. At the same time the

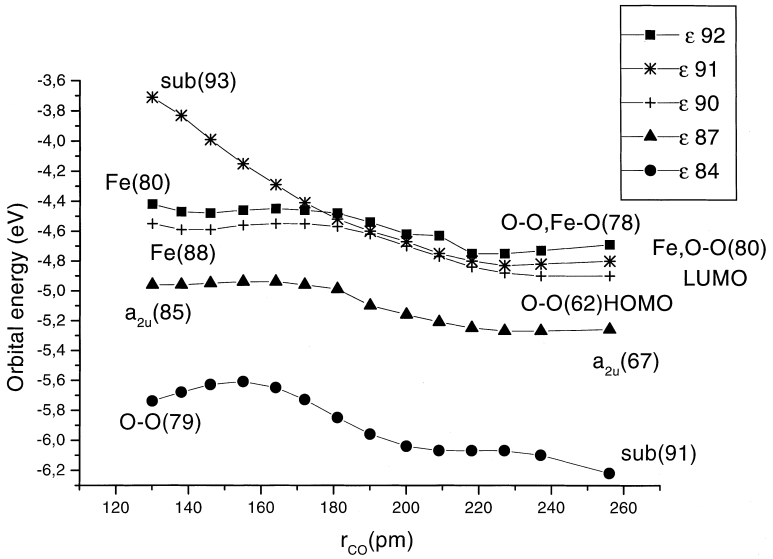

Fig. 7. Walsh diagram of the interacting spin-down molecular orbitals of the substrate-porphyrin system for the reaction of fluorobenzene hydroxylation at the para-position with respect to F with cysteinate-type coordinated peroxo-iron, as a function of the C–O distance.

O_1–O_2 orbital stabilizes further to the MO no. 84 at the end of the reaction with larger O_1 eigenvectors compared to O_2 (Tables S1 and S2), indicating diminishing of the O_1–O_2 bond strength. The changes in the eigenvectors of the initially substrate orbital (MO no. 84) for the aniline hydroxylation (see Fig. 9) are similar to those obtained for the fluorobenzene hydroxylation.

LUMO^{+1} (MO no. 92) is an antibonding π^* O_1–O_2 orbital asymmetric with respect to the Fe-O_2 plane and having a small iron contribution. Along the reaction with the diminishing of the O_1–O_2 eigenvectors this orbital transforms to an iron orbital. At the same time the π^* O_1–O_2 orbital stabilizes further stepwise to the MO no. 85 and becomes occupied in the course of the reaction. This filling of the O_1–O_2 orbital is from the HOMO substrate orbital. The stabilization of the antibonding π^* O_1–O_2 orbital in the occupied region is the main reason for the O_1–O_2 bond cleavage. At a value of 178 pm (fluorobenzene) and 180 pm (aniline) of the reaction coordinate MO no. 92 exchanges its position with MO no. 91. Taking into account the gradual change in the orbital character the numbering 91 and 92 in Table S1, S2 (fluorobenzene), Table S2, Fig. 6 (aniline) is preserved nevertheless this position exchange. Both O_1–O_2 orbitals (MO no. 90 and MO no. 92) show opposite direction of movement when compared with the substrate orbital. They are strongly stabilized at the end of the reaction to MO no. 84 and no. 85, respectively.

The LUMO of the whole system (MO no. 91) is an iron $3d_{xz,yz}$ orbital with small admixture of O_1–O_2. Along the reaction coordinate with the increase of the substrate eigenvectors the iron contribution becomes replaced by O_1–O_2 contribution. This change from iron to O_1–O_2 character with the increased parallel substrate contribution is connected with the opposite way of O_1–O_2 orbitals movement, namely stabilization as well as with the fact that the O_1–O_2 orbitals are always in interaction with the substrate orbital. Later with the further increase of the substrate content gradually all the other eigenvectors diminish and at the end of the reaction this is a substrate orbital. The changes in the eigenvectors for this MO along the reaction coordinate are presented on Fig. 10 (aniline hydroxylation). As it was already discussed above with the position

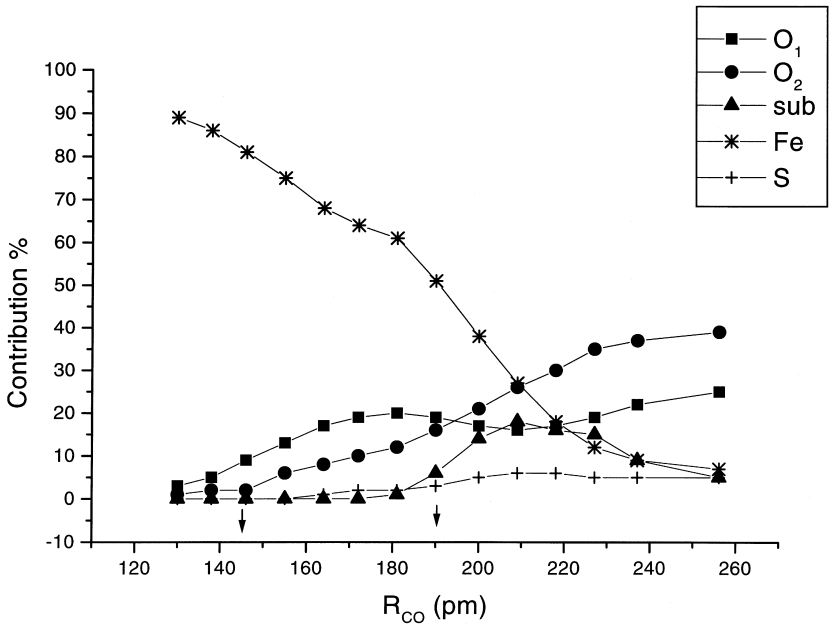

Fig. 8. Changes in the eigenvectors along the reaction pathway for the MO no. 90-hydroxylation reaction of aniline with the cysteinate-type coordinated peroxo-iron. The arrow at reaction coordinate 190 pm indicates the maximum in the potential curve for the reaction of aniline hydroxylation with cysteinate-type coordinated peroxo-iron and the arrow at 145 pm indicates the minimum in the corresponding potential curve.

exchange of MO no. 91 and no. 92 the latter is a substrate orbital showing the strong substrate destabilization from MO no. 84 to MO no. 92. This interchange of the LUMO (MO no. 91) and $LUMO^{+1}$ (MO no. 92) is the reason for the intersection of both orbitals in the Walsh diagrams, (Fig. 7, fluorobenzene hydroxylation), (Fig. 6, aniline hydroxylation).

Some other orbitals are also involved in this process. There is a hint of a_{2u} participation. The substrate content in a_{2u} decreases along the reaction coordinate together with the increase of the a_{2u} participation (Tables S1 and S2). The MO no. 89 is also indirectly involved by showing the transformation from iron to O_1–O_2 orbital on the way of the O_1–O_2 orbital stabilization.

The analysis of the orbital interactions reveals that the specific reaction mechanism for this hydroxylation process catalyzed by the peroxo-iron is quite different from the corresponding one with oxenoid-iron as a catalytic center [2,3]. The O_1–O_2 moiety has the most important role here. The two O_1–O_2 orbitals (MO no. 90 and MO no. 92 at large separation) are playing the role of substrate mediator. During the substrate destabilization the latter interacts with O_1–O_2 orbitals. The role of the iron is limited to its σ- and π- interactions which influence the strength of the O_1–O_2 bond, although the iron orbital mediates contemporary the substrate orbital when exchanging later with the π^* O_1–O_2 orbital (Tables S1 and S2). There is a small S orbital participation in all molecular orbitals on the substrate delocalization along the reaction. However, the role of the sulfur is mainly restricted to the electron donor ability of the cysteinate-group. Thiolate is the most electron-donating ligand. The π donation is promoted by two factors: (a) the extra lone pair of electrons residue in the p_x orbital of the sulfur atom, (b) the thiolate ion in these complexes tends to take an orientation which maximizes the p_x-dπ interaction and transfers π electrons to the O_1–O_2 subunit. This extra π electron density facilitates later the O_1–O_2 bond cleavage.

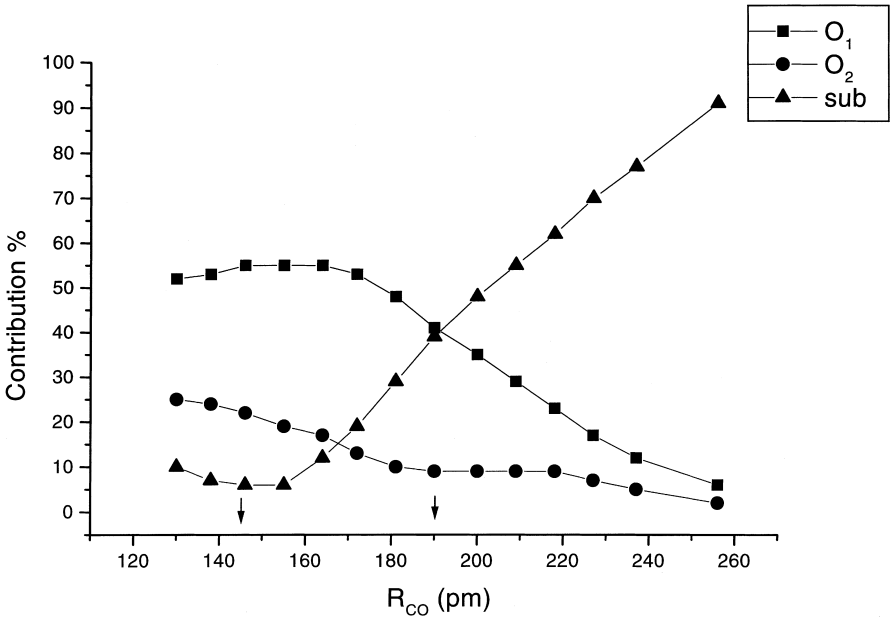

Fig. 9. Changes in the eigenvectors along the reaction pathway for the MO no. 84-hydroxylation reaction of aniline with the cysteinate-type coordinated peroxo-iron. The arrow at reaction coordinate 190 pm indicates the maximum in the potential curve for the reaction of aniline hydroxylation with cysteinate-type coordinated peroxo-iron and the arrow at 145 pm indicates the minimum in the corresponding potential curve.

6.2. Aniline hydroxylation-histidyl-type coordinated peroxo-iron

The picture of the orbital interaction is more complicated in the case of histidyl-type proximal ligand because most of the orbitals involved in the reaction are delocalized over the entire O_1–O_2, iron and the porphyrin a_{2u} orbital.

Table S3, describing the changes in orbital character is given in the supplementary material (Appendix A). The Walsh diagram is presented in Fig. 11. The orbitals involved in the reaction at large separation are the substrate π bonding orbital (MO no. 91), the MO no. 93 — an a_{2u} orbital, the MO no. 95 — a mixed iron and O_1–O_2 orbital, the HOMO of the whole system (MO no. 96) — an iron $3d_{xz,yz}$ orbital, the LUMO (MO no. 97), an O_1–O_2 orbital as well as iron $3d_{xz}$ and LUMO^{+1} (MO no. 98) an O_1–O_2 orbital with iron $3d_{xz,yz}$ admixture. Again the O_1–O_2 orbitals are playing an important role as substrate mediator.

During destabilization the substrate orbital (MO no. 91) has participation in MO no. 93, MO no. 96, MO no. 97 and at a reaction coordinate of 209 pm where MO no. 97 and 98 exchange their position (Table S3) in MO no. 98. In other words, the substrate destabilizes from MO no. 91 to MO no. 98 and becomes unoccupied in the course of the reaction.

The O_1–O_2 orbitals (MO no. 97 and no. 98 at large separation) have an opposite way of movement, namely they show stabilization. The MO no. 97 stabilizes to MO no. 91 along the reaction pathway with higher O_1 eigenvectors when compared with those of O_2. The MO no. 98 which at large separation participates also and in MO no. 93 stabilizes in the course of the reaction in the occupied region to MO no. 92.

The role of a_{2u} is augmented in this case of a histidyl-type axial ligand. As a result of an inner electron-density redistribution, mentioned also in [44], the a_{2u} orbital is not completely filled. The a_{2u} orbital no. 93 has 57% a_{2u} content at large

separation. With the diminishing of the substrate participation along the reaction coordinate the a_{2u} eigenvectors increase to approximately 92% at the end of the reaction.

The secondary role of iron is connected with the small iron contribution in all orbitals during the substrate's destabilization and its participation in the process is mainly restricted to the possible σ- and π-interactions with the O_1–O_2 moiety.

The orbitals of the histidyl-type axial ligand are strongly stabilized and again their role is restricted to the possible σ- and π-interactions with the iron and via iron with the O_1–O_2 moiety already discussed above.

7. Conclusions

The reaction mechanism for the hydroxylation reactions of substituted aromatic substrates, namely fluorobenzene and aniline, catalyzed by peroxo- and hydroperoxo- intermediates have been investigated on the bases of electronic structure calculations in local spin-density approximation. The results reveal that the peroxo-iron intermediate in addition to the oxenoid-iron, as has been shown in our previous calculations [2,3], also is an active oxidant for these hydroxylation reactions, but not the hydroperoxy-iron. Potential curves have been calculated with different mutual orientations of the catalytic center and the substrate in order to find arrangement enabling the primary reaction step.

The following results for the reaction pathway and the mechanism have been obtained.

Non-repulsive potential curves are obtained only with peroxo-iron as a catalytic center, but not with hydroperoxo-iron.

Stronger attractive interaction together with stabilization of the whole system is obtained when the projection of the O_1–O_2 bond on the porphyrin plane lies on the bisector of the N_1FeN_2 angle.

The mutual substrate-porphyrin orientation with dihedral angle between the plane of the substrate and the porphyrin plane of 45° is more favorable compared with the parallel orientation between these two planes. This leads to the stabilization of the whole system by more than 40 kcal/mol. This orientation for the case of fluorobenzene hydroxylation differs from the one obtained by us for the same reaction but catalyzed by the oxenoid-iron [2].

The specific reaction mechanism obtained for the hydroxylation process of substituted aromatic substrates, catalyzed by the peroxo-iron is quite different from the mechanism by the oxenoid-iron as a catalytic center [2,3]. The decisive role in this process has the O_1–O_2 moiety; the O_1–O_2 orbitals act as electron mediator. On its way of destabilization the substrate HOMO orbital always interacts with O_1–O_2 orbitals. The partial electron transfer from the substrate to the peroxo-iron populates the π^* antibonding O_1–O_2 orbital which along the reaction pathway stabilizes very strong in the occupied region. These two factors, namely population of an antibonding orbital and its strong stabilization in the occupied region are the main reasons for the O_1–O_2 bond rupture. An additional reason is the O_1–O_2 eigenvectors ratio in the initially substrate orbital. At the end of the reaction the later is an O_1–O_2 orbital where the eigenvectors for O_1 are substantially higher compared with those of O_2 (Tables S1, S2 and S3). The role of the iron and the axial ligand is restricted to the possible σ- and π-interactions. In the case of the cysteinate-type axial ligand its electron donating effect to the iron facilitates later the π back-donation from Fe to the antibonding O_1–O_2 orbital which additionally makes the O_1–O_2 bond rupture easier.

Taking into account the potential curves obtained for the reactions of aniline hydroxylation catalyzed by cysteinate- and histidyl-type coordinated peroxo-iron (Fig. 3b and Fig. 4) together with the calculated electron flow during the reaction in both cases we can conclude that the histidyl-type coordinated peroxo-iron is also a good catalytic intermediate. The reaction profiles represent the effectiveness of the histidyl-type coordinated peroxo-iron involved in P450 types of hydroxylation reactions.

Our calculations show that the electron flow

Table S1
Energies (in eV) and character (in percent) of the spin − down orbitals involved in the reaction of fluorobenzene with the cysteinate − type coordinated peroxo − iron (attack on para − position with respect to F

r_{OC}	e_{84}	Sub	O_1	O_2	e_{87}	a_{2u}	S	O_1	Fe	O_2	Sub	e_{89}	O_1	Fe	O_2		
256	−6.22	91	6	1	−5.26	67	1	4	7	15	2	−4.98	6	77	9		
237	−6.10	63	13	4	−5.27	71	2	2	7	11	4	−5.00	7	74	11		
227	−6.07	56	18	6	−5.27	74	1	1	6	8	6	−5.01	9	70	13		
218	−6.07	48	24	8	−5.25	77	0	0	6	6	5	−4.99	13	63	17		
209	−6.07	42	31	8	−5.21	79	0	0	5	4	5	−4.95	18	55	20		
200	−6.04	36	37	8	−5.16	81	0	0	5	3	5	−4.88	24	46	24		
190	−5.96	29	45	8	−5.10	82	0	0	4	2	5	−4.83	32	37	26		
181	−5.85	21	51	10	−5.04	83	1	1	4	1	5	−4.80	40	28	26		
172	−5.73	14	56	12	−4.99	84	2	3	3	0	4	−4.80	45	24	25		
164	−5.65	10	59	15	−4.96	84	2	6	2	0	2	−4.81	50	21	25		
155	−5.61	7	59	18	−4.94	84	2	7	3	0	1	−4.86	54	15	25		
146	−5.63	5	59	20	−4.95	83	2	8	2	1	0	−4.93	59	10	26		
138	−5.68	6	58	21	−4.96	84	3	7	2	1	0	−5.04	62	5	26		
130	−5.74	8	57	22	−4.96	85	3	6	2	1	0	−5.16	64	3	25		
r_{OC}	e_{90}	S	O_1	Fe	O_2	Sub	e_{91}	S	O_1	Fe	O_2	Sub	e_{92}	S	O_1	Fe	O_2
256	−4.90	5	25	6	37	7	−4.80	14	5	69	6	0	−4.69	1	38	17	43
237	−4.90	5	22	7	35	11	−4.82	13	7	64	9	1	−4.73	2	36	23	39
227	−4.88	5	19	10	33	16	−4.83	11	11	56	14	2	−4.75	3	32	30	33
218	−4.84	5	16	16	29	19	−4.80	7	18	41	22	5	−4.75	6	24	44	23
209	−4.77	5	16	26	25	18	−4.75	4	22	26	27	12	−4.63	10	16	57	14
200	−4.70	4	17	37	20	14	−4.67	2	20	16	26	23	−4.62	11	11	65	9
190	−4.62	3	19	51	15	7	−4.60	2	16	8	22	38	−4.54	12	8	70	5
181	−4.57	2	19	63	10	1	−4.52	2	10	5	17	50	−4.48	12	6	71	4
172	−4.55	2	18	67	8	0	−4.41	1	6	2	12	65	−4.46	13	5	75	2
164	−4.55	1	16	70	7	0	−4.29	1	3	1	7	85	−4.45	13	4	77	2
155	−4.56	1	13	75	5	0	−4.15	0	2	1	5	90	−4.46	14	3	78	0
146	−4.59	0	10	80	3	0	−3.99	0	1	1	4	93	−4.48	14	2	79	1
138	−4.59	0	6	85	2	0	−3.83	0	0	1	4	94	−4.47	15	1	80	0
130	−4.55	0	3	88	0	0	−3.71	0	0	1	4	93	−4.42	15	1	80	0

Table S2
Energies (in eV) and character (in percent) of the spin − down orbitals involved in the reaction of aniline with the cysteinate − type coordinated peroxo − iron (attack on para − position with respect to NH_2)

r_{OC}	e_{84}	O_1	O_2	Sub	e_{87}	a_{2u}	O_1	O_2	Fe	Sub	e_{89}	O_1	Fe	O_2
256	−5.97	6	2	91	−5.17	70	3	13	7	2	−4.88	6	78	9
237	−5.87	12	5	77	−5.17	74	1	6	10	5	−4.89	7	75	11
227	−5.86	17	7	70	−5.16	76	1	5	7	6	−4.89	9	71	13
218	−5.86	23	9	62	−5.13	79	0	5	5	7	−4.86	12	64	16
209	−5.87	29	9	55	−5.09	80	0	5	4	6	−4.80	17	57	20
200	−5.84	35	9	48	−5.03	82	0	4	3	6	−4.72	22	49	23
190	−5.76	41	9	39	−4.96	82	0	4	2	6	−4.65	29	40	25
181	−5.65	48	10	29	−4.90	83	1	4	1	6	−4.61	34	37	24
172	−5.53	53	13	19	−4.86	83	3	3	0	5	−4.62	42	28	26
164	−5.44	55	17	12	−4.83	82	6	2	0	3	−4.63	47	22	26
155	−5.41	55	19	6	−4.81	82	8	2	0	1	−4.69	53	15	26
146	−5.42	55	22	6	−4.81	82	9	1	2	1	−4.77	59	9	27
138	−5.44	53	24	7	−4.81	82	8	1	2	0	−4.87	63	4	27
130	−5.47	52	25	10	−4.79	84	7	1	2	0	−5.00	62	2	25

r_{OC}	e_{90}	S	O_1	Fe	O_2	Sub	e_{91}	S	O_1	Fe	O_2	Sub	e_{92}	S	O_1	Fe	O_2
256	−4.80	5	25	7	39	5	−4.70	14	5	69	7	0	−4.59	1	39	16	44
237	−4.78	5	22	9	37	9	−4.71	13	8	64	10	1	−4.62	2	36	21	40
227	−4.75	5	19	12	35	15	−4.70	11	11	56	14	2	−4.63	3	33	29	35
218	−4.70	6	17	18	30	16	−4.66	7	18	40	23	5	−4.61	6	25	42	25
209	−4.62	6	16	27	26	18	−4.60	4	22	26	29	13	−4.54	9	17	55	16
200	−4.54	5	17	38	21	14	−4.52	3	21	16	29	24	−4.46	11	12	63	10
190	−4.45	3	19	51	16	6	−4.43	2	17	8	26	39	−4.37	12	9	68	7
181	−4.39	2	20	61	12	1	−4.33	3	12	8	21	51	−4.31	12	8	67	6
172	−4.38	2	19	64	10	0	−4.20	2	8	2	16	68	−4.29	13	6	75	3
164	−4.38	1	17	68	8	0	−4.04	1	4	2	10	80	−4.29	13	5	76	2
155	−4.39	0	13	75	6	0	−3.87	1	2	2	7	87	−4.29	14	3	78	1
146	−4.40	0	9	81	2	0	−371	1	1	2	5	90	−4.29	14	2	79	1
138	−4.37	0	5	86	2	0	−3.48	1	1	1	5	91	−4.24	15	1	80	0
130	−4.29	0	3	89	1	0	−3.48	1	1	1	5	91	−4.16	15	1	80	0

Table S3
Energies (in eV) and character (in percent) of the spin − down orbitals involved in the reaction of aniline with the histidyl − type coordinated peroxo − iron (attack on para − position with respect to NH_2)

r_{OC}	e_{91}	O_1	O_2	Sub	e_{93}	a_{2u}	O_1	Fe	O_2	Sub	e_{95}	O_1	Fe	O_2		
256	−7.46	15	16	63	−6.99	57	3	4	14	12	−6.86	16	56	22		
237	−7.58	20	14	59	−6.90	60	2	3	11	15	−6.79	20	47	26		
218	−7.69	28	12	54	−6.80	73	9	3	8	11	−6.71	27	38	30		
209	−7.73	33	12	45	−6.75	77	0	3	6	10	−6.69	30	33	32		
200	−7.74	39	12	40	−6.69	81	0	2	4	8	−6.67	35	27	33		
190	−7.70	45	13	31	−6.63	84	0	2	2	5	−6.64	41	20	35		
181	−7.64	51	14	24	−6.57	87	0	1	1	4	−6.63	48	13	35		
172	−7.54	55	16	17	−6.53	88	1	1	0	3	−6.63	54	9	34		
164	−7.46	58	18	11	−6.49	91	2	1	0	2	−6.64	58	6	32		
155	−7.44	60	21	10	−6.46	91	2	0	0	1	−6.68	61	4	30		
146	−7.39	60	22	9	−6.44	91	3	0	0	0	−6.75	40	1	18		
138	−7.38	59	23	9	−6.42	92	3	0	0	0	−6.83	66	0	27		
130	−7.41	57	24	11	−6.40	92	2	0	0	0	−6.94	67	1	25		
r_{OC}	e_{96}	O_1	Fe	O_2	Sub	a_{2u}	e_{97}	O_1	Fe	O_2	Sub	a_{2u}	e_{98}	O_1	Fe	O_2
256	−6.78	3	69	7	5	10	−6.75	14	23	23	11	26	−6.63	32	30	35
237	−6.69	2	79	4	4	5	−6.65	16	15	27	17	23	−6.56	29	38	30
218	−6.58	0	89	1	2	2	−6.52	16	7	30	26	18	−6.48	25	48	23
209	−6.54	0	90	0	0	1	−6.44	14	7	30	32	0	−6.44	23	48	23
200	−6.50	0	91	0	0	0	−6.36	13	6	28	40	0	−6.42	21	59	16
190	−6.43	0	91	0	0	0	−6.25	10	6	24	46	0	−6.36	17	67	11
181	−6.34	0	91	0	0	0	−6.14	8	6	20	59	0	−6.29	12	75	7
172	−6.28	0	91	0	0	0	−6.02	5	5	14	71	0	−6.23	9	80	5
164	−6.22	0	91	0	0	0	−5.88	3	4	10	81	0	−6.18	7	83	3
155	−6.15	0	91	0	0	0	−5.76	2	3	7	90	0	−6.11	5	86	2
146	−6.07	0	92	0	0	0	−5.68	1	2	6	90	0	−6.04	4	88	1
138	−6.00	0	92	0	0	0	−5.61	1	1	6	91	0	−5.94	2	90	1
130	−5.84	0	92	0	0	0	−5.45	1	1	7	91	0	−5.82	2	91	0

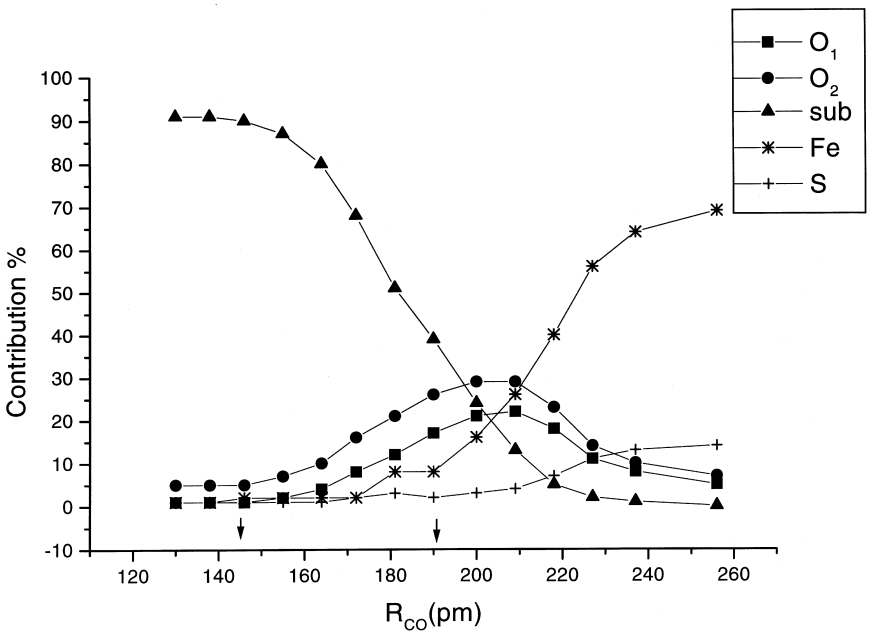

Fig. 10. Changes in the eigenvectors along the reaction pathway for the MO no. 91-hydroxylation reaction of aniline with the cysteinate-type coordinated peroxo-iron. At a reaction coordinate of approximately 180 pm the MO no. 91 and no. 92 exchange their position (as already mentioned in the text). The arrow at reaction coordinate 190 pm indicates the maximum in the potential curve for the reaction of aniline hydroxylation with cysteinate-type coordinated peroxo-iron and the arrow at 145 pm indicates the minimum in the corresponding potential curve.

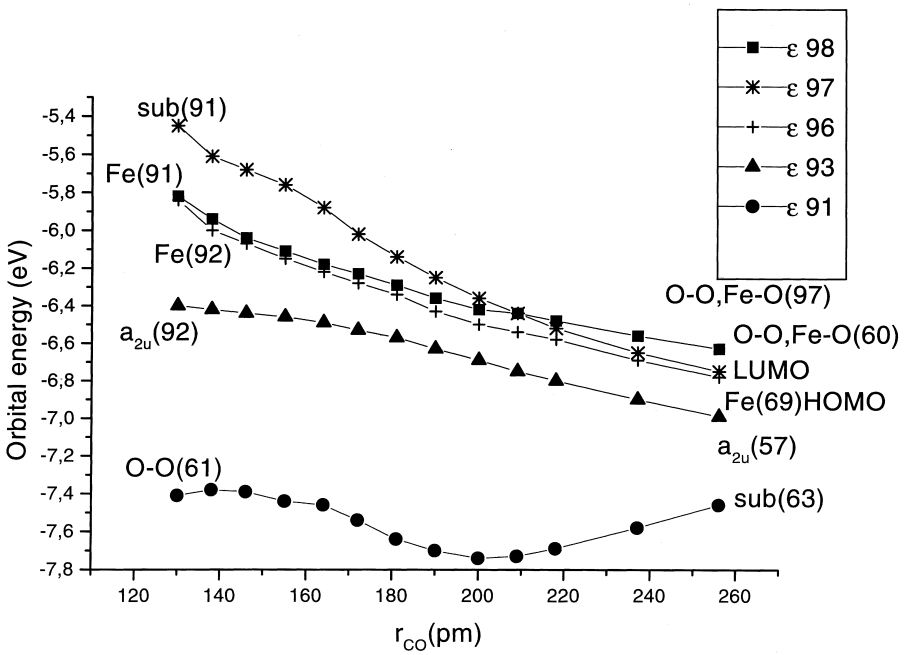

Fig. 11. Walsh diagram of the interacting spin-down molecular orbitals of the substrate-porphyrin system for the reaction of aniline hydroxylation at the para-position with respect to NH_2 with histidyl-type coordinated peroxo-iron, as a function of the C–O distance.

towards the peroxo-iron catalytic center is strongly reduced when compared with the same reaction but catalyzed with oxenoid-iron [2,3].

In all the cases studied irrespective of the substrate and the nature of the axial ligand, the potential curves reach a minimum at approximately 130–140 pm, expressing the length of an aromatic C–O bond.

References

[1] M. Sono, M.P. Roach, E.D. Coulter, J.H. Dawson, Heme-containing oxygenases, Chem. Rev. 96 (1996) 2841–2887.

[2] O. Zakharieva, M. Grodzicki, A.X. Trautwein, C. Veeger, I.M.C.M. Rietjens, Molecular orbital study of the hydroxylation of benzene and monofluorobenzene catalysed by iron-oxo porphyrin π cation radical complexes, J. Biol. Inorg. Chem. 1 (1996) 192–204.

[3] O. Zakharieva, M. Grodzicki, A.X. Trautwein, C. Veeger, I.M.C.M. Rietjens, Molecular orbital study of porphyrin-substrate interactions in cytochrome P450 catalysed aromatic hydroxylation of substituted anilines, Biophys. Chem. 73 (1998) 189–203.

[4] V. Dorovska-Taran, M.A. Posthumus, S. Boeren et al., Oxygen exchange with water in heme-oxo intermediates during H_2O_2-driven oxygen incorporation in aromatic hydrocarbons catalyzed by microperoxidase-8, Eur. J. Biochem. 253 (1998) 659–668.

[5] M.J.H. van Haandel, J.-L. Primus, C. Teunis et al., Reversible formation of high-valent iron-oxo porphyrin intermediates in heme-based catalysis: revisiting the kinetic model for horseradish peroxidase, Inorg. Chim. Acta 275-276 (1998) 98–105.

[6] J.T. Groves, Key elements of the chemistry of cytochrome P450. The oxygen rebound mechanism, J. Chem. Educ. 62 (1985) 928–931.

[7] J.T. Groves, Y. Watanbe, T.J. McMurry, Oxygen activation by metalloporphyrins. Formation and decomposition of an acylperoxymanganese (III) complex, J. Am. Chem. Soc. 105 (1983) 4489–4490.

[8] R.H. Holm, Metal-centered oxygen atom transfer reactions, Chem. Rev. 87 (1987) 1401–1449.

[9] S. Kobayashi, M. Nakano, T. Goto, T. Kimura, A.P. Schaap, An evidence of the peroxidase-dependent oxygen transfer from hydrogen peroxide to sulfides, Biochem. Biophys. Res. Commun. 135 (1986) 166–171.

[10] T. Egawa, H. Shimada, Y. Ishimura, Evidence for compound I formation in the reaction of cytochrome P450cam with m-chloroperbenzoic acid, Biochem. Biophys. Res. Commun. 201 (1994) 1464–1469.

[11] I. Schlichting, J. Berendzen, K. Chu, et al. Crystal structures of intermediates occuring along the reaction pathway of cytochrome $P450_{cam}$, Fed. Am. Soc. Exp. Biol. J. 11 (1997) A769.

[12] J.H. Dawson, M. Sono, Cytochrome P-450 and chloroperoxidase: thiolate-ligated heme enzymes. Spectroscopic determination of their active site structures and mechanistic implications of tiolate ligation, Chem. Rev. 87 (1987) 1255–1276.

[13] M. Momenteau, C.A. Reed, Synthetic heme dioxygen complexes, Chem. Rev. 94 (1994) 659–698.

[14] J.H. Dawson, Probing structure-function relations in heme-containing oxygenases and peroxidases, Science 24 (1988) 433–439.

[15] D. Mansuy, P. Battioni, J.-P. Battioni, Chemical model systems for drug-metabolizing cytochrome-P-450-dependent monooxygenases, Eur. J. Biochem. 184 (1989) 267–285.

[16] M. Schappacher, L. Ricard, J. Fisher et al., Synthesis, structure and spectroscopic properties of the two models for the active site of the oxygenated state of cytochrome P450, Eur. J. Biochem. 168 (1987) 419–429.

[17] E. McCanlish, A.R. Miksztal, M. Nappa, A.Q. Sprenger, J.S. Valentine, Reactions of superoxide with iron porphyrins in aprotic solvents. A high spin ferric porphyrin peroxo complex, J. Am. Chem. Soc. 102 (1980) 4268–4271.

[18] P.A. Cole, C.H. Robinson, Mechanistic studies on a placental aromatase model reaction, J. Am. Chem. Soc. 113 (1991) 8130–8137.

[19] A.L. Balch, The reactivity of spectroscopically detected peroxy complexes of iron porphyrins. Inorg. Chim. Acta 198-200 (1992) 297–307.

[20] J.H. Dawson, R.H. Holm, J.R. Trudell et al., Oxidized cytochrome P-450. Magnetic circular dichroism evidence for thiolate ligation in the substrate-bound form. Implication for the catalytic mechanism, J. Am. Chem. Soc. 98 (1976) 3707–3709.

[21] T.L. MacDonald, L.T. Burka, S.T. Wright, F.P. Guengerich, Mechanisms of hydroxylation by cytochrome P-450: exchange of iron-oxygen intermediates with water, Biochem. Biophys. Res. Commun. 104 (1982) 620–625.

[22] A.D.N. Vaz, D.F. McGinnity, M.J. Coon, Epoxidation of olefins by cytochrome P450: Evidence from site-specific mutagenesis for hydroperoxo-iron as an electrophilic oxidant, Proc. Natl. Acad. Sci. USA 95 (1998) 3555–3560.

[23] A.D.N. Vaz, S.J. Pernecky, G.M. Raner, M.J. Coon, Peroxo-iron and oxenoid-iron species as alternative oxygenating agents in cytochrome P450-catalyzed reactions. Switching by threonine-302 to alanine mutagenesis of cytochrome P450 2B4, Proc. Natl. Acad. Sci. USA 93 (1996) 4644–4648.

[24] A.D.N. Vaz, E.S. Roberts, M.J. Coon, Olefin formation in the oxydative deformylation of aldehydes by cytochrome P-450. Mechanistic implications for catalysis by oxygen-derived peroxide, J. Am. Chem. Soc. 113 (1991) 5886–5887.

[25] E.S. Roberts, A.D.N. Vaz, M.J. Coon, Catalysis by cytochrome P-450 of an oxidative reaction in xenobiotic aldehyde metabolism: deformylation with olefin formation, Proc. Natl. Acad. Sci. USA 88 (1991) 8963–8966.

[26] A.D.N. Vaz, K.S. Kessel, M.J. Coon, Aromatization of a bicyclic steroid analog, 3-oxodecalin-4-ene-10-carboxaldehyde, by liver microsomal cytochrome P450 2B4, Biochemistry 33 (1994) 13651–13661.

[27] A.M. Osman, J. Koerts, M.G. Boersma, S. Boeren, C. Veeger, I.M.C.M. Rietjens, Microperoxidase/H_2O-catalyzed aromatic hydroxylation proceeds by a cytochrome P-450-type oxygen-transfer reaction mechanism, Eur. J. Biochem. 240 (1996) 232–238.

[28] M. Grodzicki, A self-consistent-charge Xα method. I. Theory, J. Phys. B 13 (1980) 2683–2692.

[29] D. Habibollanhzadeh, M. Grodzicki, J.M. Seminaro, P. Politzer, A computational study of the concerted triple dissociation of 1,3,5-triazacyclohexane and its 1,3,5-trinitro derivative (RDX), J. Phys. Chem. 95 (1991) 7702–7966.

[30] M. Grodzicki, J.M. Seminaro, P. Politzer, Energy barriers of symmetry forbidden reactions: local density functional calculations, J. Chem. Phys. 94 (1991) 1668–1669.

[31] J.P. Dahl, J. Avery (Eds.), Local Density Approximations in Quantum Chemistry and Solid State Physics, Plenum Press, New York, 1984.

[32] R.G. Parr, W. Yang, Density-Functional Theory of Atoms and Molecules, Oxford University Press, New York, 1989.

[33] J.K. Labanowski, J.W. Andzelm (Eds.), Density Functional Methods in Chemistry, Springer, New York, 1991.

[34] J. Antony, M. Grodzicki, A.X. Trautwein, Local density functional study of oxoiron (IV) porohyrin complexes and their one-electron oxidized derivatives. Axial ligand effects, J. Phys. Chem. A 101 (1997) 2692–2701.

[35] I.M.C.M. Rietjens, A.E.M.F. Soffers, C. Veeger, J. Vervoort, Regioselectivity of cytochrome P-450 catalyzed hydroxylation of fluorobenzenes predicted by calculated frontier orbital substrate characteristics, Biochemistry 32 (1993) 4801–4812.

[36] N.H.P. Cnubben, J. Vervoort, C. Veeger, I.M.C.M. Rietjens, Study on the regioselectivity and mechanism of the aromatic hydroxylation of monofluoroanilines, Chem. Biol. Int. 85 (1992) 151–172.

[37] M.J. Frish et al., Gaussian 98, Revision A.5, Gaussian, Inc, Pittsburgh, PA, 1998.

[38] J.H. Dawson, L.-S. Kau, J.E. Penner-Hahn et al., Oxygenated cytochrome P-450-cam and chloroperoxidase: direct evidence for sulfur donor ligation trans to dioxygen and structural characterization using EXAFS spectroscopy, J. Am. Chem. Soc. 108 (1986) 8114–8116.

[39] A. Dedieu, M.-M Rohmer, A. Veillard, Ab initio calculations of metalloporphyrins, Adv. Quant. Chem. 16 (1982) 43–95.

[40] A. Author, in: K.M. Hellwege, A.M. Hellwege (Eds.), Landolt–Boernstein: Numerical Data and Functional Relationships in Science and Technology (New series), II/7, Springer, Berlin, 1900.

[41] K.R. Korzekwa, W.F. Trager, M. Gouterman, D. Spangler, G.H. Loew, Cytochrome P450 mediated aromatic oxidation: a theoretical study, J. Am. Chem. Soc. 107 (1985) 4273–4279.

[42] D. Mansuy, P. Battioni, Diversity of reactions catalyzed by heme-thiolate proteins, in: K.M. Kadish, K.M. Smith, R. Guilard (Eds.), The Porphyrin Handbook, 4, , 1999, pp. 1–15.

[43] K. Nakamoto, H. Oshio, Effect of thiolate vs. nitrogen-base ligands on O_2 stretching frequencies of (oxytetraphenylporphyrinato) cobalt, J. Am. Chem. Soc. 107 (1985) 6518–6521.

[44] T. Ogura, S. Hitora, D.A. Proshlyakov, K. Schinzawa-Itoh, S. Yoshikawa, T. Kitagawa, Time-resolved resonance Raman evidence for tight coupling between electron transfer and proton pumping of cytochrome *c* oxidase upon the change from the Fe^{V} oxidation level to the Fe^{IV} oxidation level, J. Am. Chem. Soc. 118 (1996) 5443–5449.